RAPID COMMUNICATIONS

PHYSICAL REVIEW B VOLUME 47, NUMBER 15 15 APRIL 1993-I

Direct atomic structure by multiple-energy inversion of experimental forward-scattering-photoelectron and Auger-electron-diffraction data

Hua Li and S. Y. Tong
Laboratory for Surface Studies and Department of Physics, University of Wisconsin–Milwaukee, Milwaukee, Wisconsin 53201

D. Naumovic, A. Stuck, and J. Osterwalder
Institut de Physique, Universite de Fribourg, 1700 Fribourg, Switzerland
(Received 29 December 1992)

We demonstrate multiple-wave-number reconstruction of experimental data for forward-scattering-photoelectron and Auger-electron-angular-diffraction distributions of Cu(001). Direct structural information of the nearest- and next-nearest-neighbor atoms is obtained. The structure so determined provides a useful starting point for refinement by diffraction methods, thus avoiding the cumbersome trial-and-error process.

We demonstrate the inversion of multiple-energy forward-scattering-photoelectron and Auger-electron-diffraction data to determine the surface structure of Cu(001). Szöke[1] and Barton[2] have recently pointed out the analogy between photoelectron and Auger-electron diffraction and point-source electron holography. This leads to the possibility of directly inverting electron-diffraction data to obtain structural information in real space. In the forward-scattering geometry, it is necessary to use multiple-wave-number phase locking[3–8] to invert photoelectron and Auger-electron-diffraction distributions for emission from bulk samples. In this paper, we present experimental results which demonstrate the realization of these ideas using forward-scattering data measured at 11 energies from 643 to 1736 eV for Cu(001). The method of reconstruction is based on the small-window energy-extension process (SWEEP).[3–7] The forward-scattering data for Cu(001) were taken by laboratory-based apparatus using a combination of Auger and x-ray photoemission spectroscopy (XPS) emission lines (see Table I).[9,10] These data provide a stringent test of the reconstruction method because they contain a mixture of initial states and excitation matrix elements.

The large-solid-angle data at 11 energies are shown from left to right in ascending order of energy in Fig. 1.

TABLE I. Experimental XPS and Auger transitions for Cu(001).

Kinetic energy (eV)	Transition	Excitation
643.0	Cu 2*s*	Si $K\alpha$
768.0	Cu *LMM*	Mg $K\alpha$
807.5	Cu 2*p*	Si $K\alpha$
838.9	Cu *LMV*	Mg $K\alpha$
918.6	Cu *LVV*	Mg $K\alpha$
1131.3	Cu 3*s*	Mg $K\alpha$
1178.0	Cu 3*p*	Mg $K\alpha$
1250.7	Cu 3*d*	Mg $K\alpha$
1617.7	Cu 3*s*	Si $K\alpha$
1664.2	Cu 3*p*	Si $K\alpha$
1736.6	Cu 3*d*	Si $K\alpha$

The highest-energy data are shown in the central panel. The most striking features in these $\hat{\mathbf{k}}$-space maps are the bright forward-focusing spots due to zeroth-order interference between the direct and scattered waves along internuclear directions.[11–15] From these focusing spots, all internuclear directions in the surface region can be mapped out. In the inset, we show the high-density crystallographic directions for a bulk-terminated Cu(001) surface.

The SWEEP method utilizes the fact that the internuclear directions are already given by the $\hat{\mathbf{k}}$-space focusing peaks to within an accuracy of 1°–3°. It also recognizes the fact that the interference fringes within a small angular cone Ω_j of a focusing direction $\hat{\mathbf{R}}_j$ are dominated by the first and in some cases second interference oscillations from atoms in that particular internuclear direction. The SWEEP method, therefore, restricts the range of data inversion to a small cone with a half-angle of about 30°–40° around a focusing direction. The inversion process is repeated for other focusing directions. Phase-shift and scattering amplitude effects are corrected by a function defined as[16]

$$p_j(k_n\hat{\mathbf{k}})=f(k_n\hat{\mathbf{k}}\cdot\hat{\mathbf{R}}_j)+|f(k_n\hat{\mathbf{k}}\cdot\hat{\mathbf{R}}_i)|+\cdots\ , \tag{1}$$

where $f(k_n\hat{\mathbf{k}}\cdot\hat{\mathbf{R}}_j)$ is the scattering factor along the $\hat{\mathbf{R}}_j$ direction and $f(k_n\hat{\mathbf{k}}\cdot\hat{\mathbf{R}}_i)$ for $i\neq j$ are scattering factors along nearby focusing directions. If the angular cone Ω_j is small, it is sufficient to include in Eq. (1) the scattering direction $\hat{\mathbf{R}}_j$ and the *closest* neighbor focusing direction only. In the SWEEP method,[3–7] a phase factor is used to phase-lock Fourier transforms at different wave numbers:

$$\phi^j_{R_i}(\mathbf{R})=\left|\sum_{n=1}^{N}e^{-ik_nR_i}F^j_{k_n}(\mathbf{R})\right|^2\ , \tag{2}$$

where[7]

$$F^j_{k_n}(\mathbf{R})=\int_{\Omega_j}\frac{\chi(k_n\hat{\mathbf{k}})e^{i\mathbf{k}_n\cdot\mathbf{R}}}{p_j(k_n\hat{\mathbf{k}})\cos\theta}dk_{n,x}dk_{n,y}\ . \tag{3}$$

In Eq. (3), $\chi(k_n\hat{\mathbf{k}})$ is the normalized data at wave number

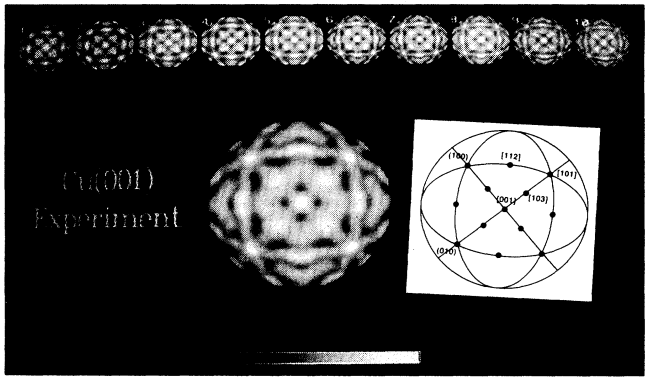

FIG. 1. Hemispherical XPS and Auger data at 11 energies from left to right in ascending order of energies corresponding to Table I. The inset shows the bulk Cu(001) crystallographic directions.

k_n and the integral is taken over a small angular cone Ω_j around focusing direction $\hat{\mathbf{R}}_j$. Equations (2) and (3) are applied to the experimental data shown in Fig. 1. For demonstration, we select two focusing directions for image reconstruction: A nearest-neighbor close-packed direction [101] and a next-nearest-neighbor direction [001]. From the data in Fig. 1, the [101] focusing spot is determined at 46°–48° from normal, the [103] spot at 19°–20° from normal, and the [001] spot is at the normal direction. These experimentally determined focusing

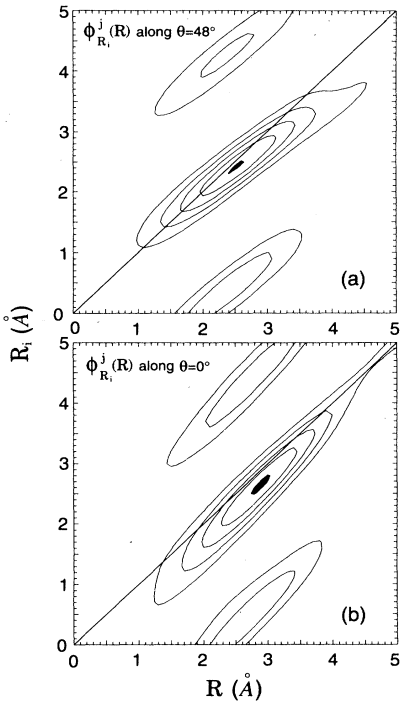

FIG. 2. Contour plots of $\phi^j_{R_i}(R)$ along (a) $\theta=48°$ and (b) $\theta=0°$ focusing directions. The contour levels are from 0 to 250, in steps of 50.

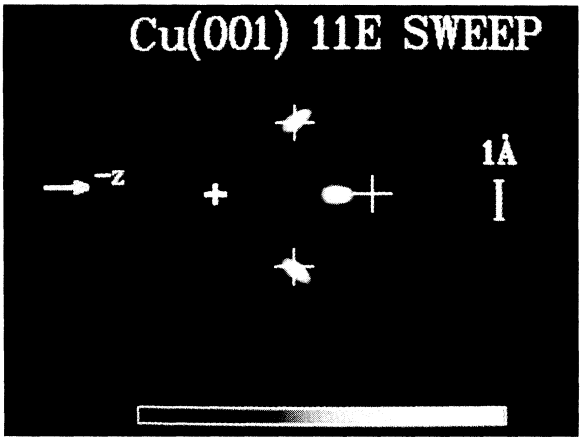

FIG. 3. Reconstructed image using SWEEP along the [101], [001], and [$\bar{1}$01] directions, with 10° half-angular cones in real space. Data at 11 energies shown in Fig. 1 are used. The plane of view is (010).

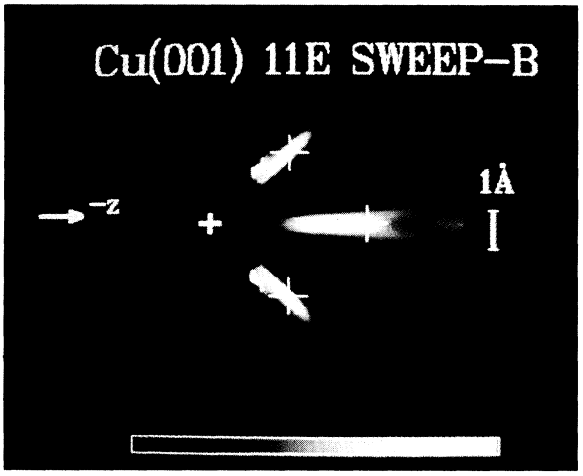

FIG. 4. Reconstructed image using SWEEP-B, i.e., Barton's phase. Other conditions are the same as in Fig. 3.

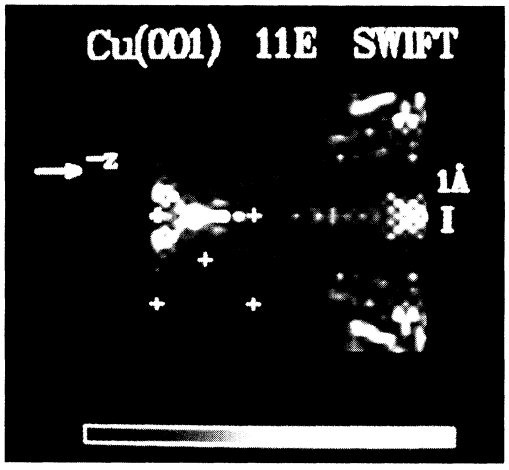

FIG. 5. Reconstructed image using the SWIFT method from data at 11 energies shown in Fig. 1, using the entire 156° window. The plane of view is (010). The image is dominated by artifacts. Little intensity is present at atomic positions (marked by crosses).

directions are compared to the bulk crystallographic directions of 45°, 18.4°, and 0°, respectively. The interference fringes in an angular cone with 30° half-angle are used around each experimentally determined focusing direction. For the phase-shift correction, we use $f(k_n\hat{\mathbf{k}}\cdot\hat{\mathbf{R}}_{48°})$ and $|f(k_n\hat{\mathbf{k}}\cdot\hat{\mathbf{R}}_{20°})|$ in the sum of Eq. (1) for the [101] direction and $f(k_n\hat{\mathbf{k}}\cdot\hat{\mathbf{R}}_{0°})$ and four rotation-symmetric $|f(k_n\hat{\mathbf{k}}_n\cdot\hat{\mathbf{R}}_{20°})|$ in the sum for the [001] direction.

To determine the optimal phase in Eq. (2), we substitute trial values R_i in Eq. (2) and evaluate $\phi^j_{R_i}(R)$ with R along the $\hat{\mathbf{R}}_{48°}$ and $\hat{\mathbf{R}}_{0°}$ focusing directions, respectively. The two-dimensional contours of $\phi^j_{R_i}(R)$ are plotted in Figs. 2(a) and 2(b), and the maxima occur at $R_i=2.44\pm0.2$ and 2.64 ± 0.3 Å, respectively, for the two directions. Note that these maxima lie away from the $R_i=R$ line, indicating that the propagator's phase in the near-field Green's function $G^+_{L'L}(\mathbf{R})$ deviates from that of the far-field exponential form of e^{ik_nR}. Substituting each optimal R_i value in Eqs. (2) and (3), the multiple-wave-number reconstructed images are shown in Fig. 3 where the plane of view is normal to the surface [i.e., the (010) plane] and it passes through the copper nuclei. In this figure, real-space images along the [001], [101], and its mirror direction [$\bar{1}$01] are shown. Since the integral in Eq. (3) includes interference oscillations restricted to a small angular cone Ω_j, the reconstruction is not expected to produce meaningful structural information at directions far from $\hat{\mathbf{R}}_j$. Also, the correction function $p_j(k_n\hat{\mathbf{k}})$ is designed to correct for the scattering phase and amplitude of atoms along the $\hat{\mathbf{R}}_j$ direction only. Therefore, we have restricted the image reconstruction to cones in real space with half-angle 10° around each of the three focusing directions. In Fig. 3, the small cross marks the position of an emitting atom and the large crosses mark the bulk positions of nearest-neighbor atoms along [101] and [$\bar{1}$01] as well as the next-nearest-neighbor atom along [001]. The images, which are bright and essentially free of artifacts, appear near the bulk Cu atom positions.

Barton[8] has proposed a multiple-wave-number reconstruction method in which the near-field phase factor of $G^+_{LL'}(\mathbf{R})$ is set equal to the far-field form of e^{ik_nR}. Using this phase factor, Eq. (2) becomes

$$\phi^j(\mathbf{R})=\left|\sum_{n=1}^{N} e^{-ik_nR}F^j_{k_n}(\mathbf{R})\right|^2 . \quad (4)$$

We have incorporated Barton's phase in the SWEEP method, using the same phase-shift correction function and small angular cone as before. We apply the SWEEP-B (i.e., Barton) method to the identical data set and the results are shown in Fig. 4, where the plane of view is again (010). Bright spots, elongated in the emitter-to-scatterer directions, again correspond well with the positions of the crosses for the nearest-neighbor and next-nearest-neighbor atoms. Figures 3 and 4 show that either inversion method provides direct structural information for the nearest- and next-nearest-neighbor atoms, although the accuracy is only ~0.5 Å. Furthermore, using Barton's phase, the images have larger full widths at half-magnitudes.

Two ingredients in the SWEEP method are worth noting. (i) In order to control artifacts, the self-interference term must be small compared to the image term. If a large-solid-angle database is used in the forward-scattering geometry, the many focusing directions included in the database contribute to a large self-interference term:

$$\chi(k_n\hat{\mathbf{k}})_{\text{self}}\sim\frac{|f(k_n\hat{\mathbf{k}}\cdot\hat{\mathbf{R}}_j)|^2}{R^2_{j1}}+\frac{|f(k_n\hat{\mathbf{k}}\cdot\hat{\mathbf{R}}_i)|^2}{R^2_{i1}}+\cdots . \quad (5)$$

This term is highly peaked along each focusing direction, and the strong angular anisotropy (i.e., rapidly varying function of $\hat{\mathbf{k}}$) destroys the stationary-phase condition required for high-fidelity wave-front reconstruction. In the SWEEP method, the self-interference term is small because only a single focusing direction is included and this term is further reduced by the division of $f(k_n\hat{\mathbf{k}}\cdot\hat{\mathbf{R}}_j)$. (ii) The purpose of dividing $\chi(k_n\hat{\mathbf{k}})$ by a scattering factor is to cancel a similar factor contained in $\chi(k_n\hat{\mathbf{k}})$. The SWEEP method achieves this cancellation by restricting $\chi(k_n\hat{\mathbf{k}})$ to fringes produced primarily by atoms in a particular focusing direction $\hat{\mathbf{R}}_j$. The division of $\chi(k_n\hat{\mathbf{k}})$ by $f(k_n\hat{\mathbf{k}}\cdot\hat{\mathbf{R}}_j)$ indeed produces a stationary-phase condition within this restricted angular cone in the single-scattering limit.

We tested the requirement for using a small-window database by inverting the same 11 energy data shown in Fig. 1 except we used data covering the entire angular space (approximately 156°). In the inversion process, we either used no phase-shift correction (i.e., following the algorithm proposed by Barton[8,17]) or we used a generalized scattering-factor correction $f(\hat{\mathbf{k}}\cdot\hat{\mathbf{R}})$ as suggested by Hardcastle *et al.* in the SWIFT algorithm.[18] In both cases, the brightest intensity streaks in the reconstructed images were artifacts which appeared near the origin and along the [001] direction. These artifacts were caused by the strong self-interference terms in Eq. (5) and the lack of proper cancellation of the anisotropic scattering factors.[10] The transformed image of the 11 energy data by the SWIFT method[18] is shown in Fig. 5. The bright artifacts near the origin and along [001] overwhelmed any intensities located near the correct atomic positions (marked by crosses). The fidelity of the images shown in Figs. 3 and 5, which were inverted from the same set of data, showed that the SWEEP method did a much better job at controlling artifacts.

In summary, the small-window inversion method SWEEP, using either optimized phases $e^{ik_nR_i}$ for each focusing direction or Barton's phase e^{ik_nR}, has been demonstrated for multiple-energy forward-scattering experimental XPS and Auger data. The advantage of the forward-scattering geometry is that multiple-energy diffraction data can be measured without using synchrotron radiation. Data inversion by SWEEP is a direct method and the structure so determined can be refined by diffraction methods without using other trial geometries.

This work was supported in part by U.S. ONR Grant No. N00014-90-J-1749 and the Fonds National Suisse pour la Recherche Scientifique.

[1]A. Szöke, in *Short Wavelength Coherent Radiation: Generation and Applications,* edited by D. T. Attwood and J. Boker, AIP Conf. Proc. No. 147 (AIP, New York, 1986).

[2]J. J. Barton, Phys. Rev. Lett. **61**, 1356 (1988).

[3]S. Y. Tong, H. Huang and Hua Li, in *Advances in Surface and Thin Film Diffraction,* edited by T. C. Huang, P. I. Cohen, and D. J. Eaglesham, MRS Symposia Proceedings No. 208 (Materials Research Society, Pittsburgh, 1991), p. 13.

[4]H. Huang, Hua Li, and S. Y. Tong, Phys. Rev. B **44**, 3240 (1991).

[5]S. Y. Tong, H. Huang, and C. M. Wei, Phys. Rev. B **46**, 2452 (1992).

[6]S. Y. Tong, Hua Li, and H. Huang, Phys. Rev. Lett. **67**, 3102 (1991).

[7]S. Y. Tong, Hua Li, and H. Huang, Phys. Rev. B **46**, 4155 (1992).

[8]J. J. Barton, Phys. Rev. Lett. **67**, 3106 (1991); J. J. Barton and L. J. Terminello, in *The Structure of Surfaces III,* edited by S. Y. Tong, M. A. Van Hove, X. Xie, and K. Takayanagi (Springer, Berlin, 1991).

[9]A. Stuck, D. Naumovic, H. A. Aebischer, T. Greber, J. Osterwalder, and L. Schlapbach, Surf. Sci. **264**, 380 (1992).

[10]A. Stuck, D. Naumovic, T. Greber, J. Osterwalder, and L. Schlapbach, Surf. Sci. **274**, 441 (1992); D. Naumovic, A. Stuck, T. Greber, J. Osterwalder, and L. Schlapbach, Phys. Rev. B **47**, 7462 (1993).

[11]W. F. Egelhoff, Jr., Phys. Rev. B **30**, 1051 (1984).

[12]H. C. Poon and S. Y. Tong, Phys. Rev. B **30**, 6211 (1984).

[13]S. A. Chambers, in *Advances in Physics,* edited by S. Doniach (Taylor and Francis, London, 1991).

[14]C. S. Fadley, in *Synchrotron Radiation Research: Advances in Surface Science,* edited by R. Z. Bachrach (Plenum, New York, 1990).

[15]S. Y. Tong, M. W. Puga, H. C. Poon, and M. L. Xu, in *Chemistry and Physics of Solid Surfaces VI,* edited by R. Vanselow and R. Howe (Springer, New York, 1986).

[16]S. Y. Tong, C. M. Wei, T. C. Zhao, H. Huang, and Hua Li, Phys. Rev. Lett. **66**, 60 (1991).

[17]L. J. Terminello, J. J. Barton, and D. A. Lapiano-Smith, J. Vac. Sci. Technol. B **10**, 2088 (1992).

[18]S. Hardcastle, Z. L. Han, G. R. Harp, J. Zhang, B. L. Chen, D. K. Saldin, and B. P. Tonner, Surf. Sci. **245**, L190 (1991).

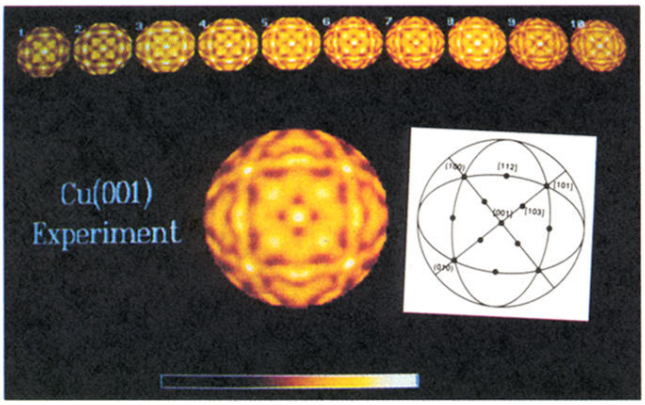

FIG. 1. Hemispherical XPS and Auger data at 11 energies from left to right in ascending order of energies corresponding to Table I. The inset shows the bulk Cu(001) crystallographic directions.

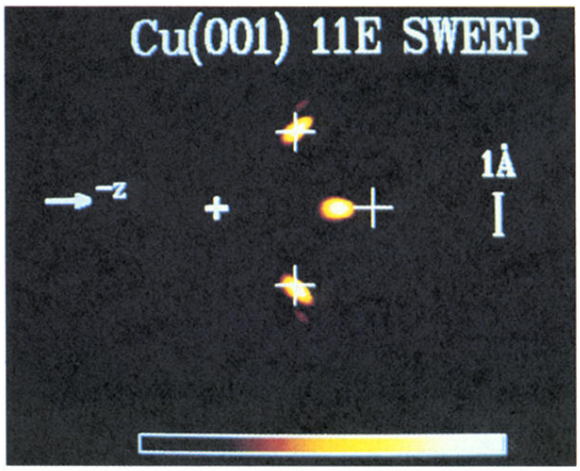

FIG. 3. Reconstructed image using SWEEP along the [101], [001], and [$\bar{1}$01] directions, with 10° half-angular cones in real space. Data at 11 energies shown in Fig. 1 are used. The plane of view is (010).

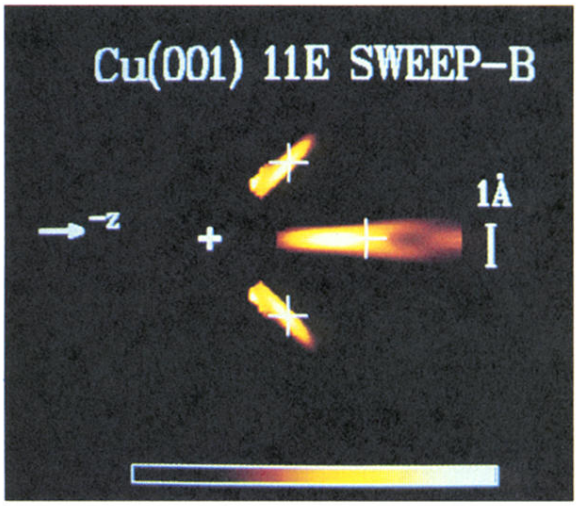

FIG. 4. Reconstructed image using SWEEP-B, i.e., Barton's phase. Other conditions are the same as in Fig. 3.

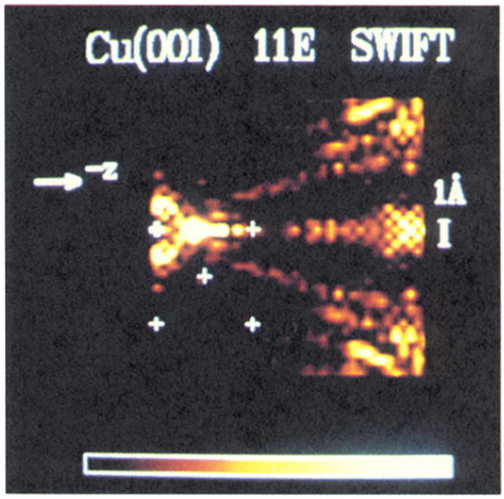

FIG. 5. Reconstructed image using the SWIFT method from data at 11 energies shown in Fig. 1, using the entire 156° window. The plane of view is (010). The image is dominated by artifacts. Little intensity is present at atomic positions (marked by crosses).